Rare Met. (2021) 40(7):1897–1906
https://doi.org/10.1007/s12598-020-01481-7

RARE METALS

ORIGINAL ARTICLE

Microstructures and mechanical properties of a cast Al–Cu–Li alloy during heat treatment procedure

Shu-Wei Duan, Kenji Matsuda, Tao Wang*, Yong Zou*

Received: 15 March 2019 / Revised: 17 April 2019 / Accepted: 29 May 2020 / Published online: 27 August 2020

Abstract Al–Cu–Li alloy is a huge potential alloy for aerospace industry due to its low density and excellent comprehensive performances. In this study, the microstructures and mechanical properties of a novel cast Al–Cu–Li alloy during the heat treatment were investigated. Results showed that most of the secondary phases along grain boundaries in as-cast state were dissolved into the Al matrix after homogenization and solution treatment, while the Cu-rich phases were slightly segregated once again on grain boundaries after aging. A relatively good combination of strength and ductility (average ultimate tensile strength of 430 MPa and elongation of 8.9%) was obtained after natural aging. Transmission electron microscopy (TEM) results revealed that there was a complicated precipitate distribution in this cast alloy after natural aging. Compared with the similar alloys which introduced dislocations before aging, the density of T_1 (Al_2CuLi) phases was decreased but the size was increased. The low volume fraction of δ′ phase, medium density of needle-shaped precipitates and relativity narrow precipitates-free zone with varying widths near grain boundary are the reasons accounting for the improvement of performances.

S.-W. Duan, T. Wang*, Y. Zou*
MOE Key Laboratory for Liquid–Solid Structure Evolution and Materials Processing, Institute of Materials Joining, Shandong University, Jinan 250061, China
e-mail: wxm689wxm@sdu.edu.cn

Y. Zou
e-mail: yzou@sdu.edu.cn

K. Matsuda
Department of Materials Science and Technology, Faculty of Engineering, University of Toyama, Toyama 930-8555, Japan

Keywords Al–Cu–Li alloy; Heat treatment; Microstructure; Mechanical property; Precipitate

1 Introduction

The lithium (Li) element, as the lightest metal in the world, was added into the aluminum (Al) alloy; it not only greatly reduced the density of alloy, but also obtained excellent comprehensive performances. The third generation of Al–Cu–Li alloy has been extensively used as structural material for aerospace industry and attracted many researchers to study various aspects of them. The precipitates, especially T_1 (Al_2CuLi) and θ′ (Al_2Cu), in this kind of alloy played vital roles on its superior performances [1–5].

In recent years, most studies related to Al–Cu–Li alloy are mainly focused on two aspects: (1) relationship of microstructure evolution and mechanical properties; (2) the structure and formation mechanism of various precipitates during their evolution. The first aspect was almost specialized in rolled or wrought state due to that they are the actual states of alloy application, but when it comes to the second aspect, researchers seemed not to be very concerned about the state of alloy. For example, in the study of the growth mechanism of T_1 precipitate, rolled alloy was employed in Refs. [6, 7], while in Refs. [8, 9] cast alloy was used. Besides, some scholars directly introduced the dislocation into the as-cast alloy by pre-stretching in their researches, such as Gumbmann et al. [10]. However, whether the state of the alloy would affect the behavior of precipitates is a question worthwhile to be further explored.

Casting Al–Cu–Li alloys can be used to manufacture many complex-shaped products simply, and it is of great practical value for aviation industry due to their low

density. Previous studies [11] have shown that the dislocation could greatly promote the nucleation of T_1 precipitate and suppress the width of precipitates-free zone (PFZ) in the grain boundary. However, the cast products are not allowed via pre-strength or rolling before aging considering its complex shape. Therefore, it is more reasonable to improve the performances merely using the heat treatment process.

Up to now, few researches concentrated on improving the performance of cast Al–Cu–Li alloys through the heat treatment procedure directly. Chen et al. [12] studied the heat treatment of cast Al–3Li–1.5Cu–0.2Zr alloy, and the ultimate tensile strength (UTS) obtained was 382 MPa at peak aging, but the elongation was only 2.9%. On this basis, the microstructure and mechanical properties of cast Al–2Li–2Cu–0.5Mg–0.2Zr alloy during the heat treatment were investigated by Zhang et al. [13]; although their UTS increased to 440 MPa at peak aging, the elongation was still only 4.5%. Both of them selected high Li content in order to obtain low density, but high Li content ($\geq$ 2 wt%) may also lead to poor ductility and insufficient damage tolerance, which would restrict the application in aerospace industry due to the high requirements for toughness [1]. Therefore, reducing Li content of cast alloy to the level of the third-generation Al–Li alloys and studying the suitable heat treatment procedure are of significance.

In this study, a third generation of Al–Cu–Li cast alloy with relatively low Cu/Li ratio and complex minor alloying elements were employed. A heat treatment procedure was implemented to gain better mechanical properties, and the microstructure features were investigated. Considering there have been abundant researches on the evolution of microstructure and mechanical properties of the Al–Cu–Li alloy during its aging already, we have not paid much attention to details in the heat treatment process, but focused on three aspects: (1) effect of the heat treatment on precipitates in grain boundaries, (2) the optimal mechanical properties achieved and (3) the final precipitate characteristics obtained.

2 Experimental

The investigated material was a novel Al–Cu–Li cast alloy, its Cu/Li ratio was further reduced in order to get low density, and the composition is shown in Table 1. The heat treatment was performed by two steps: two-stage homogenization treatment and then water-quenched artificial aging followed by 6-month natural aging. The specific parameters of the heat treatment are shown in Fig. 1.

The metallography specimens were prepared according to the standard metallography procedures. The samples were etched using Keller′s etchant (2.5 vol% HNO_3 + 1.5 vol% HCL + 1 vol% HF + 95 vol% H_2O) for 30 s and then observed using optical microscope (OM, VHX-500F Keyence) and scanning electron microscope (JMS-6610LA SEM) attached energy-dispersive spectroscope (EDS). The Vickers hardness of the artificial aging for different times was measured on a DHV-1000 digital hardness tester under a load of 0.98 N and a holding time of 15 s. The standard tensile specimens were prepared after peaking artificial aging and followed by 6 months of natural aging. Then, room-temperature tensile test was performed on a WDW-100E instrument. The fractured surfaces were also examined by SEM. X-ray diffraction (XRD, Miniflex 600) was employed with the scanning ratio of 10 (°)·min^{-1}.

The 0.8-mm-thick slices were cored from the samples after peaking aging followed by natural aging and then mechanically thinned to 120 μm. Transmission electron microscopy (TEM) samples were obtained by single-jet thinning conducted with two kinds of electrolyte: one comprises 25 vol% HNO_3 and 75 vol% CH_3OH; another comprises 10 vol% $HClO_4$ + 90 vol% C_2H_5OH. The operating temperature was below 273 K. TEM micrographs, including the selected area diffraction (SAD) and bright-field (BF) images, were taken with EM-002B TEM operated at 120 kV.

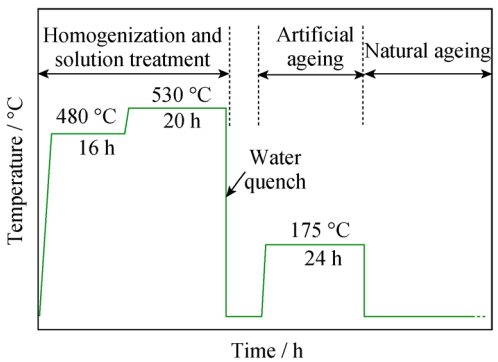

Fig. 1 Heat treatment procedures

Table 1 Chemical composition of the investigated alloy (wt%)

Cu	Li	Mn	Zr	Ti	Mg	Fe	Si	Sn	Be	Al
2.8	1.4	0.28	0.11	0.03	0.07	0.04	0.03	0.009	0.003	Bal.

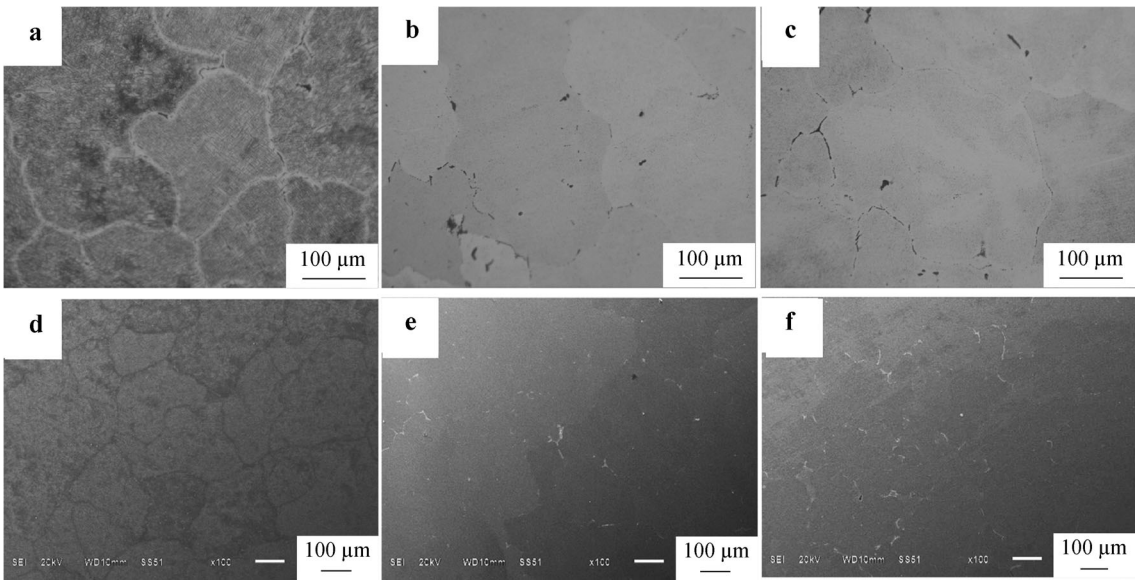

Fig. 2 **a–c** OM images and **d–f** SEM images of different stages during heat treatment: **a**, **d** as-cast alloy; **b**, **e** as-quenched alloy; **c**, **f** after aging

3 Results and discussion

3.1 Effect of heat treatment on microstructures

OM and SEM images of initial as-cast alloy are shown in Fig. 2a, d. The microstructure of as-cast alloy is characterized by explicit and wide grain boundaries. It may mean that the serious segregation of elements and secondary phases happened in there when the alloy is solidifying. Elemental map-scanning distributions in grain boundary and its neighboring areas of as-cast alloy are displayed in Fig. 3a. We can see evident Cu in grain boundaries and accompanied by partly segregation of Fe. EDS point scans in Fig. 4 further illustrate this phenomenon, it is found that

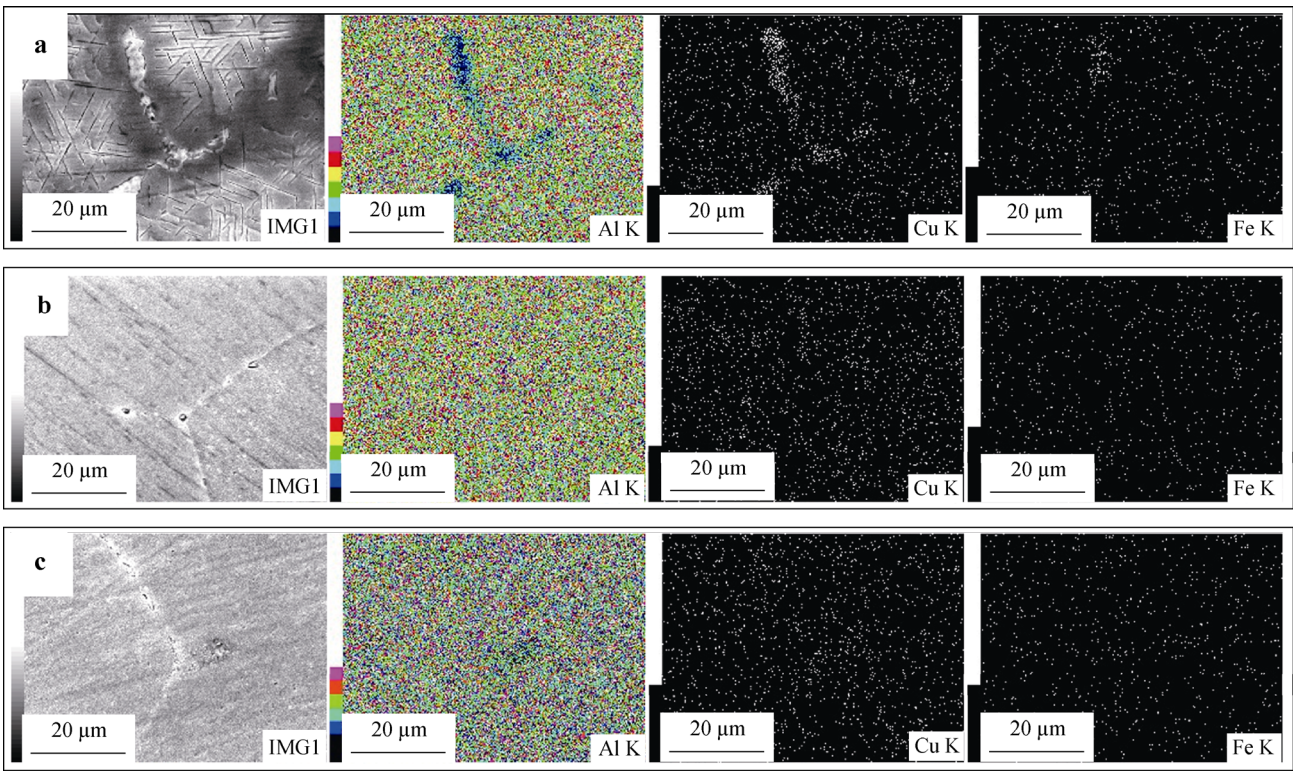

Fig. 3 Elemental map-scanning distributions of different stages during heat treatment: **a** as-cast, **b** as-quenched, and **c** after aging

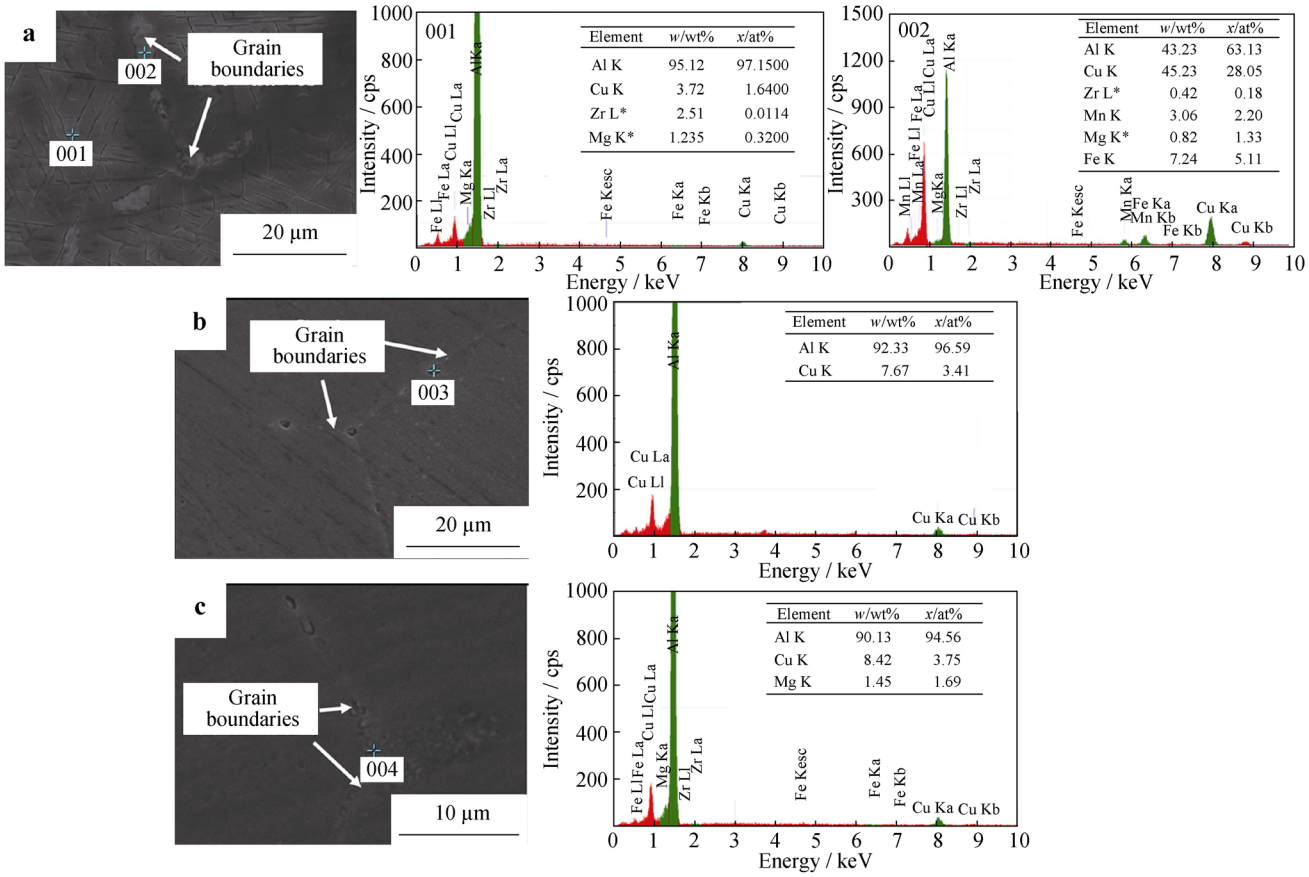

Fig. 4 EDS point scans results: **a** in grain boundary and within grain of as-cast alloy, **b** in grain boundary of as-quenched alloy, and **c** in grain boundary of after aging alloy

most microalloying elements are segregated to some extent on grain boundaries in as-cast alloy, and the content of intergranular Cu and Fe is significantly higher than the that of intragranular regions.

In order to eliminate serious segregation of elements and secondary phases constituents in the as-cast alloy meanwhile making the alloying elements be dissolved into the matrix as much as possible, two-stage homogenization and solution treatment were employed. OM and SEM images of as-quenched alloy are presented in Fig. 2b, e. Compared to the as-cast alloy, it can be observed that the grain boundaries became relatively clean and only a little amount of second phases remained. Elemental map-scanning distributions of samples after homogenization shown in Fig. 3b also illustrate the result of the homogenization. The segregation of Cu and Fe in grain boundaries in as-cast alloy is also effectively decreased. The effects of homogenization and solution on elements at the grain boundaries are also verified in EDS point scans results (Fig. 4), it can be seen that Al and Cu become main elements at the grain boundary, and the content of Cu decreased from 28.5 at% (as-cast) to 3.75 at% (as-quenched). All of these responses demonstrate that the ideal result is achieved by the homogenization and solution treatment.

The samples after natural aging were studied in the same way. In the optical microstructure (Fig. 2c), the number of fine black spots and lines increases the grain boundaries, indicating that the secondary phases on grain boundaries have slightly precipitated again after aging. Similar results are also displayed in SEM image (Fig. 2f), and the white areas are slightly increased compared to the state of as-quenched. Moreover, the results of elemental map-scanning distributions (Fig. 3c) and EDS point scans (Fig. 4c) indicate that although some grain boundary precipitates occurred after aging, there is no serious segregation of alloying elements, so the precipitation at grain boundaries in aging is only in a small scale.

XRD results of the studied alloy at different heat treatment conditions are shown in Fig. 5. It can be observed that the main peaks of as-cast alloy are α-Al and Al_3Li phases. Previous studies [14] have reported that other phases such as Al_2Cu, Al_2CuMg, AlLi and Al_6CuLi_3 should also be existed in the as-cast alloy, but there are no visible peaks of these phases probably because of their

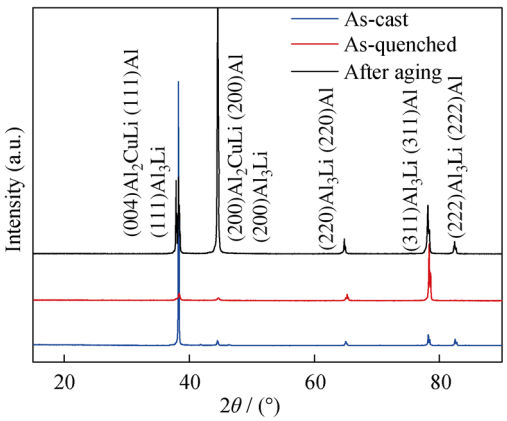

Fig. 5 XRD results of different stages during heat treatment

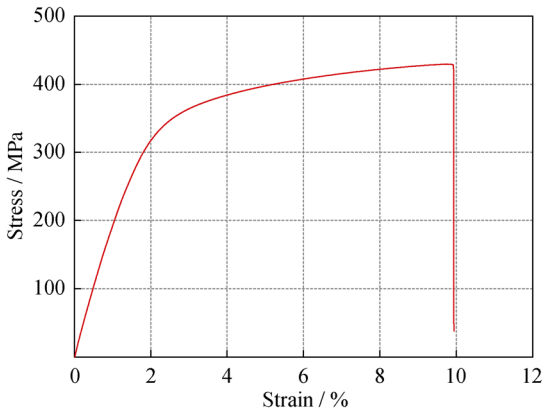

Fig. 7 Tensile properties after all treatments

relatively small amounts. The most significant aspect in this graph is the diffraction peaks of the secondary phases which declined obviously after homogenization and solution treatment, revealing that most intermetallic phases have dissolved into the Al matrix. And after aging, the T_1, θ′ and δ′ (Al_3Li) phases precipitated with a large number, and their characteristic diffraction peaks play the main role in XRD patterns.

3.2 Optimal mechanical properties achieved

Figure 6 provides the hardness evolution curve of the alloy in the process of artificial aging at 175 °C. It can be seen that the hardness increases continuously with aging time before peak aging except a slight decline in early periods of aging. The maximum hardness is occurred after aged for 24 h, and the value is ∼ HV 136. Moreover, the hardness of samples with peak-aging state can be further increased to HV 144 in subsequent 6-month natural aging. Decreus et al. [15] also observed a significant softening in the early artificial aging of 2198 and 2196 alloys. According to their research, it is mainly caused by the dissolution of solute clusters, especially Cu-rich clusters. Results of previous studies [16] have also demonstrated that the precipitation of a large amount of precipitates, such as T_1, θ′ and δ′ (Al_3Li), is directly accounted for the rapid rise of hardness subsequently, and their coarsening during over aging resulted in the decline of hardness.

The level of the eventual tensile properties after a series of heat treatments is also what we are concerned about. Figure 7 provides the engineering stress–strain curve of a representative sample after all treatments. The average UTS has achieved a relatively ideal level (430 MPa). The most significant aspect is that the mean elongation reaches 8.9%; it is a noticeable improvement compared to 2.9% or 4.5% in previous researches [12, 13]. SEM images of the fracture surface are shown in Fig. 8, and it can be seen that small and densely distributed shallow dimples are present on the fracture surface, accompanied by many smooth surfaces. It is the typical intergranular-dimple mixed-type fracture mode. The occurrence of a large amount of dimples also indicates that the relatively good ductility has been attained on the other hand.

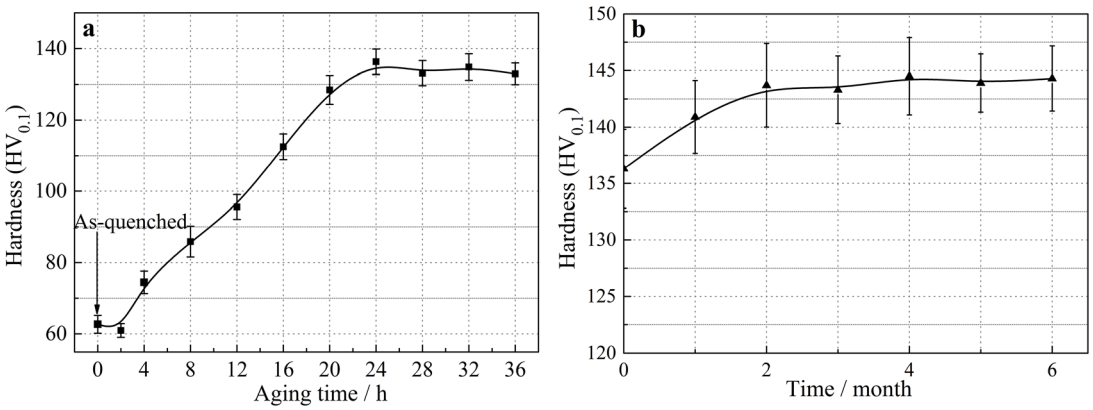

Fig. 6 Hardness evolution of studied alloy: **a** artificial aging at 175 °C and **b** natural aging of artificial peak aged alloy

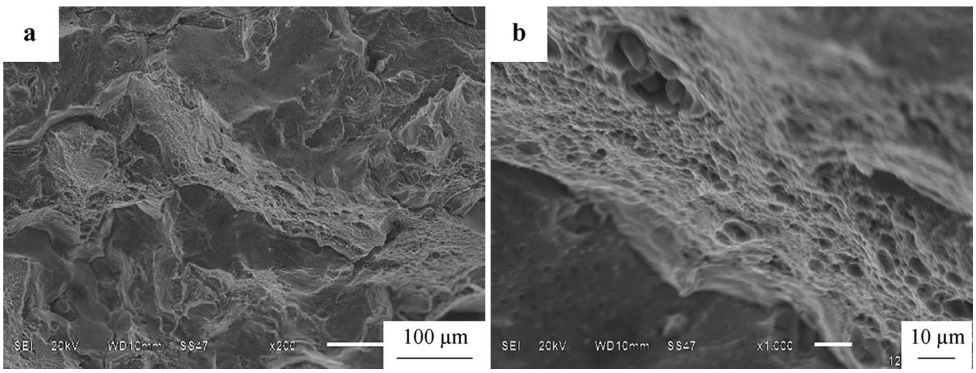

Fig. 8 SEM images of fracture surfaces of tensile sample with different magnifications

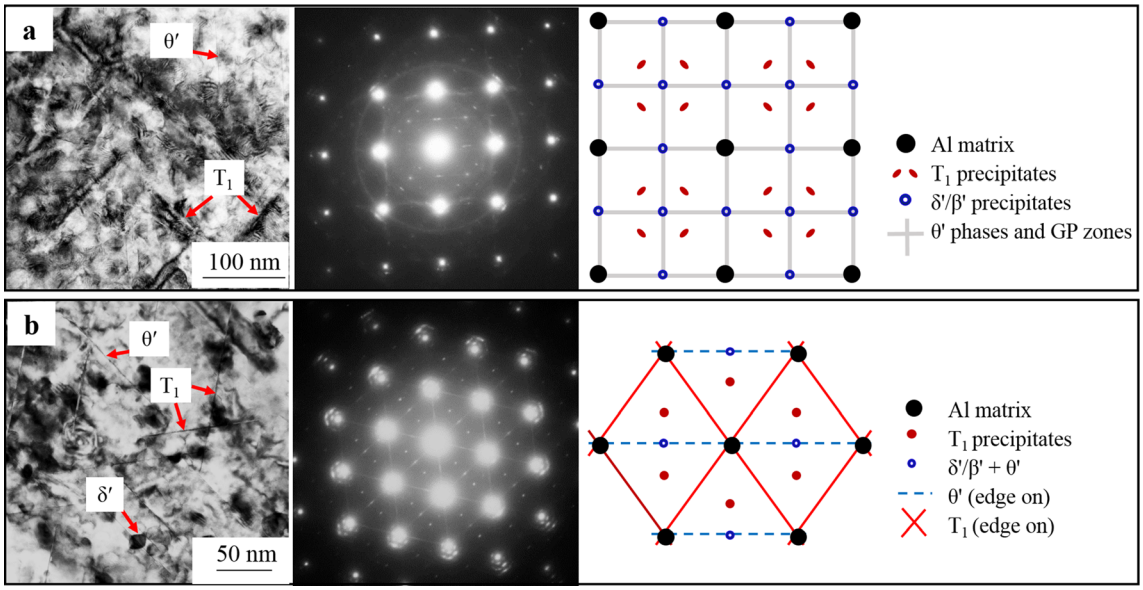

Fig. 9 BF images, SAD patterns and corresponding schematic models with **a** [100] zone axis and **b** [110] zone axis

3.3 Final precipitate features obtained

The final microstructure features of precipitates are also interesting research focus due to that the precipitates play a crucial factor in performances of Al–Cu–Li alloy. The BF images, SAD patterns and corresponding schematic models of the alloy after all treatments are given in Fig. 9. At least four sets of diffraction patterns are found, which are from the Al matrix, the T_1, θ′ and δ′ precipitates, respectively [17, 18]. These precipitates can also be explicitly observed in the BF images. The T_1 phase is hexagonal and present as platelets on Al plane [19], and θ′ phase is tetragonal and semi-coherent with the matrix, appearing as disks lying on the {100}Al planes, which are two major strengthening phases in the Al–Cu–Li alloy. The δ′ phase is spherical and may coexist with a small amount of β′ (Al_3Zr) in the form of core/shell particles [20].

In addition, other rare precipitates including the phase of the variant of θ′ and the σ ($Al_6Cu_5Mg_2$) phase are also observed. It can be seen that four orientations of needle-shaped precipitates occur in BF image of Fig. 10. Previous study [21] has clarified that two orientations belong to two variants of T_1 phase and one is regular θ′ phase with the orientation relationship of (100)θ′//(100)α and [001]θ′//[001]α in Al–Cu–Li alloy when viewing along [110]Al. However, the precipitate marked by blue line has another orientation, which is the variant of θ′ and it seems that only the direction of *c*-axis rotates 90° compared to the common θ′ phase. Two orientations of θ′ are apparent in almost all related studies of the binary Al–Cu systems when viewed in the [100] direction, such as the researches by Ma et al. [22] and Bourgeois et al. [23]. However, the θ′ variant which is perpendicular to regular θ′ phase when viewed in the [110] direction is rarely reported, and it may be due to its instability of occurrence and little amount.

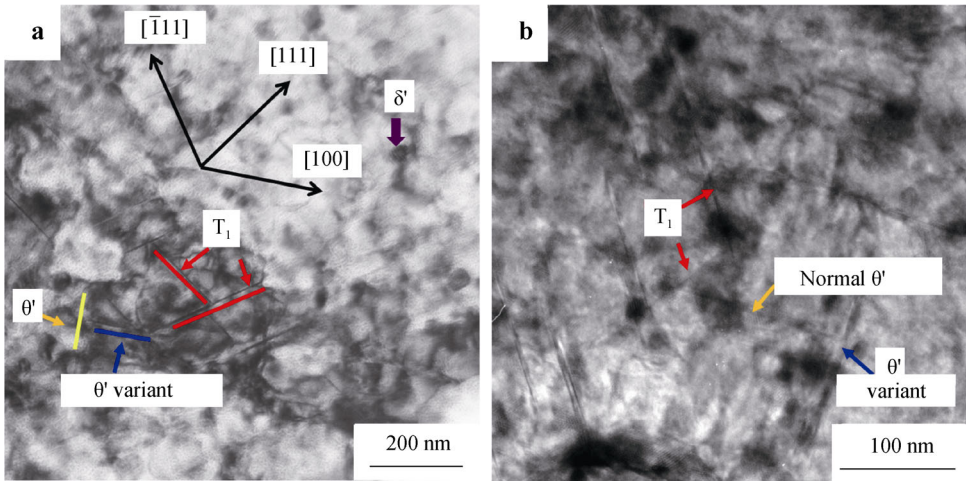

Fig. 10 TEM images of precipitate seening to θ′ variant viewed in [110] direction with different magnifications

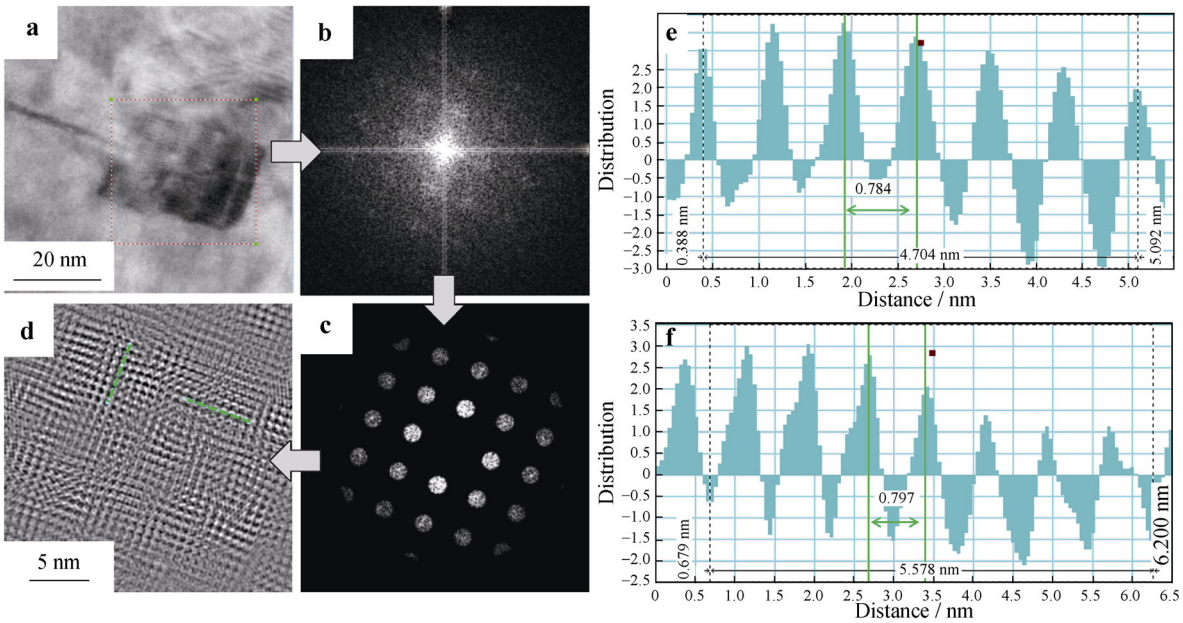

Fig. 11 **a** TEM image of σ phase viewed in [100] direction; **b** FFT image of framed area in **a**; **c** FFT image after filtering; **d** inverse FFT images; **e**, **f** corresponding image intensity contrast distribution in two vertical directions marked by green lines in **d**

Meanwhile, another phase with extremely small amount is also observed in Fig. 11. Fast Fourier transform (FFT) and inverse FFT images indicate that this phase has cubic structure and seems semi-coherent with matrix, then it is considered to be σ phase. The lattice parameters in two vertical directions of the phase are estimated to be 0.784 and 0.797 nm by spacing of image intensity, which are close to the value of 0.794 nm calculated by Li et al. [16]. Although σ phase is thought to be beneficial to the stability of the alloy due to its coarsening resistance of high temperature [24], the high concentration of Cu in σ phase may also facilitate it competing for Cu atoms with T_1 and θ′ phases in the vicinity. The area lacking of needle-shaped precipitates around σ phase as shown in Fig. 11 is not the state as we expected.

As stated above, most precipitates contained in the alloy have been expounded, but the main reason for the improvement of elongation after the natural aging is still not explicit. So, we evaluated the other information of the precipitates. The presence of large area fractions of grain boundary precipitates (GBP) and soft precipitates-free zone (PFZ) nearby is considered to be the important reason which caused the decrease in plasticity and toughness in aging aluminum alloy [25, 26]. Therefore, the TEM images of grain boundary and adjacent zone are observed, and the results are shown in Fig. 12. It can be seen that the

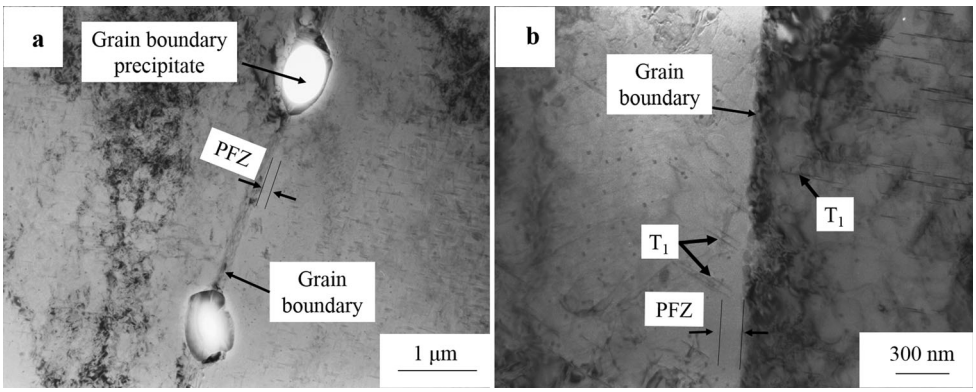

Fig. 12 TEM images around grain boundary from different views

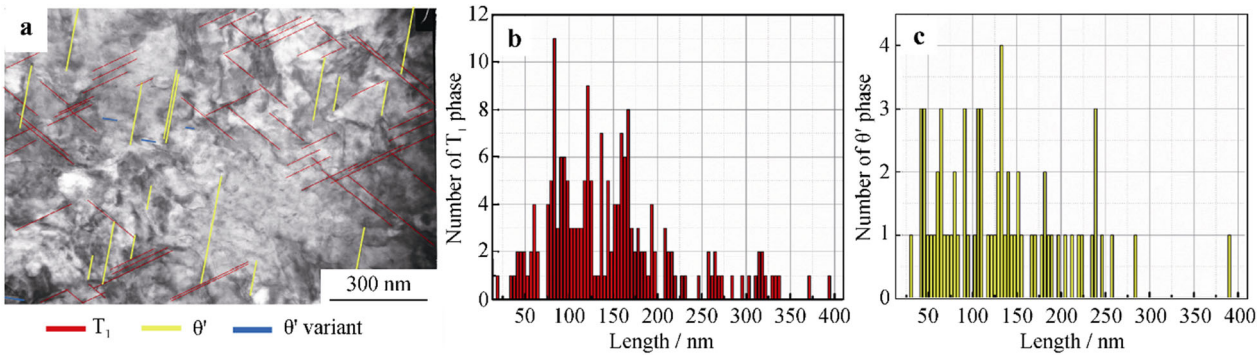

Fig. 13 **a** One of BF image for precipitates measurement viewed in [110] direction; **b** length distribution of T_1 precipitates; **c** length distribution of θ′ precipitates

relatively large GBP situates in some grain boundaries, the width of PFZ is relativity narrow and the width changes greatly with grain boundaries variation. The existence of GBP may be beneficial to facilitate the intergranular fracture, but the relativity narrow PFZ with varying widths can reduce the sensitivity of strain localization under plastic deformation; thus, it is a reason which helps to the enhancement of ductility.

In addition, the length distribution of the T_1 and θ′ precipitates in the [110] direction is estimated. As Fig. 13 shows, there is a significant difference of the distribution shape between two phases. Further calculation indicates that the average planar density of needle-shaped precipitate observed in [110]Al direction is 58.9 μm^{-2} ($T_1 \sim 43\ \mu m^{-2}$, $\theta' \sim 15.9\ \mu m^{-2}$), and the average length size of needle-shaped precipitate observed in [110]Al direction is 142.7 nm ($T_1 \sim 146.7$ nm and $\theta' \sim 131.9$ nm). Compared to related values in previous researches on rolled or pre-strength alloys (size and density information of T_1 precipitates in some studies are counted in Table 2 [11, 15, 18, 27, 28]), the average length of needle-shape precipitates is greatly increased, but the density is decreased to some extent. This may be due to the fact that

Table 2 Size and density information of T_1 precipitates in rolled Al–Cu–Li alloy

Alloy	Mean size/nm	Density information	Refs.
2198-T8	50.7	4.9 vol%	[27]
2198-T81	90	–	[28]
2196-T351	60	–	[15]
2198-T351	40	–	[15]
2195-T8	63	1696 μm^{-3}	[18]
Weldalite 049-T6	126.6	2012 μm^{-3}	[11]
Weldalite 049-T8	93.8	6392 μm^{-3}	[11]

Table 3 Size of δ′ particles in cast Al–Cu–Li alloy and corresponding mechanical properties

Alloy	Average size/nm	UTS/MPa	Elongation/%	Refs.
Al–3Li–2Cu–0.2Zr	32	415	2.7	[29]
Al–2Li–2Cu–0.5Mg–0.2Zr	21.5	443	4.5	[13]

there is no introduction of dislocations, resulting in few nucleation sites in studied alloys, and leading to continuous growth in the diameter direction of precipitates during aging. It should be emphasized that though the density of strengthening precipitates in this study is not as high as that of rolled, extruded or pre-deformation Al–Cu–Li alloys, it still has a noticeable increase compared to that of the cast alloys mentioned in Refs. [12, 13, 29]. Moreover, as shown in BF image of Fig. 9b, the volume fraction and size of spheroidal δ′ particles in this research are much less than those in previous, as shown in Table 3 [13, 29], which is mainly due to relatively lower Li content in the studied alloy.

The slip behavior of dislocations in the deformation process of age-hardened Al alloy is largely depended on the precipitates in the alloy. In Al–Cu–Li alloys, shearable δ′ phase is coherent, which is considered to be helpful to planar slip. Because few slip systems are concentrated on planar slip, it may lead to local work softening with the area of cross section of the particles reducing. This strain localization can lead to the degradation of ductility [19, 30, 31]. However, the needle-shaped precipitate, such as T_1 precipitate, occurs by single shearing due to high energy cost of the secondary glide on the same slip plane, which promotes the homogenous wavy slip on numerous slip planes. So, needle-shaped precipitate is beneficial to ductility and damage tolerance of the Al–Cu–Li alloy due to that many slip systems have functioned simultaneously [32–34]. The precipitate plays a critical role in the improvement of mechanical properties considering the large grain size and no dislocations in this studied cast alloy. Therefore, low volume fraction of δ′ phase and the increase in the density of needle-shaped precipitates are other significant reasons for the improvement of ductility.

4 Conclusion

In this study, a heat treatment procedure was implemented for a novel cast Al–Cu–Li alloy. And the effects of heat treatment on microstructure, mechanical properties and the precipitates characteristics were investigated.

The heat treatment procedure is suitable for this studied Al–Cu–Li alloy. The hardness reaches HV 144 after the peak aging and subsequent natural aging. And relatively good properties of strength and ductility (average UTS of 430 MPa and elongation of 8.9%) are obtained after natural aging. The vast majority of secondary phases, especially Cu-rich phases along grain boundaries in as-cast alloy, are dissolved into the Al matrix after the homogenization and solution treatment. After aging, it was found that some secondary phases re-precipitated on a small amount of grain boundaries. The microstructure of the alloy after aging is characterized by the presence of massive T_1, θ′ and partial δ′ precipitates, and some rare precipitates including θ′ variant and σ phase also exist. Low volume fraction of δ′ phase, medium density of needle-shaped precipitates and relativity narrow PFZ with varying widths near grain boundary are the reasons which could improve the ductility.

Acknowledgements This study was financially supported by the Key Research and Development Project of Shandong Province (No. 2018CXGC0403).

References

[1] Rioja RJ, Liu J. The evolution of Al–Li base products for aerospace and space applications. Metall Mater Trans Phys Metall Mater Sci. 2012;43A(9):3325.
[2] Dursun T, Soutis C. Recent developments in advanced aircraft aluminium alloys. Mater Des. 2014;56:862.
[3] Deschamps A, Decreus B, De Geuser F, Dorin T, Weyland M. The influence of precipitation on plastic deformation of Al–Cu–Li alloys. Acta Mater. 2013;61(11):4010.
[4] Ma YL, Lin XH, Liu DY, Lu DD, Li JF. Aging precipitates, static and dynamic performance of two Al–Li alloy sheets. Chin J Rare Met. 2019;43(7):673.
[5] Yang SL, Shen J, Zhang YA, Li ZH, Li XW, Huang SH, Xiong BQ. Processing maps and microstructural evolution of Al–Cu–Li alloy during hot deformation. Rare Met. 2019;38(12):1136.
[6] Deng Y, Bai J, Wu X, Huang G, Cao L, Huang L. Investigation on formation mechanism of T-1 precipitate in an Al–Cu–Li alloy. J Alloys Compd. 2017;723:661.
[7] Yoshimura R, Konno TJ, Abe E, Hiraga K. Transmission electron microscopy study of the evolution of precipitates in aged Al–Li–Cu alloys: the theta' and T-1 phases. Acta Mater. 2003;51(14):4251.
[8] Kang SJ, Kim TH, Yang CW, Lee JI, Park ES, Noh TW, Kim M. Atomic structure and growth mechanism of T-1 precipitate in Al–Cu–Li–Mg–Ag alloy. Scr Mater. 2015;109:68.
[9] Gao Z, Liu JZ, Chen JH, Duan SY, Liu ZR, Ming WQ, Wu CL. Formation mechanism of precipitate T-1 in AlCuLi alloys. J Alloys Compd. 2015;624:22.
[10] Gumbmann E, De Geuser F, Sigli C, Deschamps A. Influence of Mg, Ag and Zn minor solute additions on the precipitation kinetics and strengthening of an Al–Cu–Li alloy. Acta Mater. 2017;133:172.
[11] Ringer SP, Muddle BC, Polmear IJ. Effects of cold work on precipitation in Al–Cu–Mg–(Ag) and Al–Cu–Li–(Mg–Ag) alloys. Metall Mater Trans A. 1995;26(7):1659.
[12] Chen A, Peng Y, Zhang L, Wu G, Li Y. Microstructural evolution and mechanical properties of cast Al–3Li–1.5Cu–0.2Zr alloy during heat treatment. Mater Charact. 2016;114:234.
[13] Zhang X, Zhang L, Wu G, Liu W, Shi C, Tao J, Sun J. Microstructural evolution and mechanical properties of cast Al–2Li–2Cu–0.5Mg–0.2Zr alloy during heat treatment. Mater Charact. 2017;132:312.
[14] Nikitin SL, Osintsev OE, Betsofen SY. Effect of heat treatment conditions on the structure and mechanical properties of a cast Al–Li–Cu aluminum alloy. Russ Metall. 2010;2010(11):1041.
[15] Decreus B, Deschamps A, De Geuser F, Donnadieu P, Sigli C, Weyland M. The influence of Cu/Li ratio on precipitation in Al–Cu–Li-x alloys. Acta Mater. 2013;61(6):2207.

[16] Li HY, Tang Y, Zeng ZD, Zheng ZQ, Zheng F. Effect of ageing time on strength and microstructures of an Al–Cu–-Li–Zn–Mg–Mn–Zr alloy. Mater Sci Eng Struct Mater Prop Microstruct Process. 2008;498(1–2):314.
[17] Dorin T, Deschamps A, De Geuser F, Weyland M. Quantitative description of the T-1 morphology and strengthening mechanisms in an age-hardenable Al–Li–Cu alloy. In: Proceedings of the 13th International Conference on Aluminum Alloys (Icaa13). Pittsburgh; 2012:1155.
[18] Shukla AK, Baeslack WA. Study of microstructural evolution in friction-stir welded thin-sheet Al–Cu–Li alloy using transmission-electron microscopy. Scr Mater. 2007;56(6):513.
[19] Csontos AA, Starke EA. The effect of inhomogeneous plastic deformation on the ductility and fracture behavior of age hardenable aluminum alloys. Int J Plast. 2005;21(6):1097.
[20] Pletcher BA, Wang KG, Glicksman ME. Experimental, computational and theoretical studies of delta' phase coarsening in Al–Li alloys. Acta Mater. 2012;60(16):5803.
[21] Zhang SF, Zeng WD, Yang WH, Shi CL, Wang HJ. Ageing response of a Al–Cu–Li 2198 alloy. Mater Des. 2014;63:368.
[22] Ma PP, Liu CH, Wu CL, Liu LM, Chen JH. Mechanical properties enhanced by deformation-modified precipitation of θ′-phase approximants in an Al–Cu alloy. Mater Sci Eng A. 2016;676:138.
[23] Bourgeois L, Dwyer C, Weyland M, Nie JF, Muddle BC. Structure and energetics of the coherent interface between the theta' precipitate phase and aluminium in Al–Cu. Acta Mater. 2011;59(18):7043.
[24] Barr SC, Rylands LM, Jones H, Rainforth WM. Formation and characteristics of coarsening resistant cubic sigma phase in Al–4.2Cu–1.6Mg–0.2Si. Met Sci J. 2014;13(8):655.
[25] Suresh S, Vasudevan AK, Tosten M, Howell PR. Microscopic and macroscopic aspects of fracture in lithium-containing aluminum alloys. Acta Metall. 1987;35(1):25.
[26] Pasang T, Symonds N, Moutsos S, Wanhill RJH, Lynch SP. Low-energy intergranular fracture in Al–Li alloys. Eng Fail Anal. 2012;22:166.
[27] Gao C, Zhu ZX, Han J, Li HJ. Correlation of microstructure and mechanical properties in friction stir welded 2198-T8 Al–Li alloy. Mater Sci Eng Struct Mater Prop Microstruct Process. 2015;639:489.
[28] Schneider JA, Nunes AC, Chen PS, Steele G. TEM study of the FSW nugget in AA2195-T81. J Mater Sci. 2005;40(16):4341.
[29] Chen AT, Wu GH, Zhang L, Zhang XL, Shi CC, Li YL. Microstructural characteristics and mechanical properties of cast Al–3Li–*x*Cu–0.2Zr alloy. Mater Sci Eng Struct Mater Prop Microstruct Process. 2016;677:29.
[30] Sanders TH, Starke EA. The effect of slip distribution on the monotonic and cyclic ductility of Al–Li binary alloys. Acta Metall. 1982;30(5):927.
[31] De PS, Mishra RS, Baumann JA. Characterization of high cycle fatigue behavior of a new generation aluminum lithium alloy. Acta Mater. 2011;59(15):5946.
[32] Kumar KS, Brown SA, Pickens JR. Effect of a prior stretch on the aging response of an Al–Cu–Li–Ag–Mg–Zr alloy. Scr Metall Mater. 1990;24(7):1245.
[33] Gayle FW, Heubaum FH, Pickens JR. Structure and properties during aging of an ultra-high strength Al–Cu–Li–Ag–Mg alloy. Scr Metall Mater. 1990;24(1):79.
[34] Costa Teixeira J, Cram DG, Bourgeois L, Bastow TJ, Hill AJ, Hutchinson CR. On the strengthening response of aluminum alloys containing shear-resistant plate-shaped precipitates. Acta Mater. 2008;56(20):6109.